Available online at www.sciencedirect.com

SciVerse ScienceDirect

Ceramics International 39 (2013) 7445–7452

CERAMICS INTERNATIONAL

www.elsevier.com/locate/ceramint

Microstructure refinement approaches of melt-grown Al_2O_3/YAG/ZrO_2 eutectic bulk

Xue-song Fu[a], Guo-qing Chen[a,*], Yu-fei Zu[a], Jun-ting Luo[b], Wen-long Zhou[a]

[a]School of Materials Science and Engineering, Dalian University of Technology, Dalian 116085, PR China
[b]State Key Laboratory of Metastable Materials Science and Technology, Yanshan University, Qinhuangdao 066004, PR China

Received 9 January 2013; received in revised form 20 February 2013; accepted 26 February 2013
Available online 14 March 2013

Abstract

Microstructure developments of melt-grown Al_2O_3/YAG/ZrO_2 ceramic bulks were investigated by controlling composition, cooling rate, heterogeneous nucleation sites and melt superheating treatment. The solidification microstructure of sample with hypereutectic composition (ZrO_2 20 mol%) is finer than that with hypoeutectic or eutectic ones. With increasing the cooling rate, microstructure of melt-grown samples develops from colony to dendrite and finally to cell. The microscopy and the components of samples vary with the melt superheating temperature and the type of heterogeneous nucleation sites. The microstructure evolutions of melt-grown Al_2O_3/YAG/ZrO_2 eutectic relate to the melt undercooling level and the solid–liquid interfaces stability.

Keywords: Eutectic ceramic; Melt superheating treatment; Microstructure evolution; Melt undercooling; Microstructure refinement

1. Introduction

In recent decade years, Al_2O_3-based eutectic oxide ceramics as a candidate of high-temperature structural materials have been investigated extensively due to their excellent performances at high temperature levels [1]. Processing techniques for the eutectic oxide ceramic mainly include laser heated floating zone [2,3], edge-defined film-fed growth [4], micro-pulling down [5] and Bridgman method [6]. The first three methods are characterized of high temperature gradients at solid–liquid interface and can obtain samples with homogenous eutectic microstructure under rapid solidification, which generally lead to fine microstructure and high strength, for instance, the Al_2O_3–YAG DSE with submicron interphase spacing microstructure can reach a flexural strength of 2 GPa [7], but the dimensions of products are usually limited to several millimeters due to extremely high thermal residual stress. The Bridgman method is suitable to prepare bulk samples because of the low temperature gradient but generally results in very low flexural strength of 200–500 MPa due to structural defects and the coarse microstructure [5,6,8,9]. The strength of the eutectic ceramics is very sensitive to the defect size because the dislocation of ceramics does not slip at ambient temperature. The flexural strength σ_f can be expressed as a function of fracture toughness K_{IC} and critical defect size a_c as follows [10,11]:

$$\sigma_f = \left[\frac{K_{IC}}{0.65\sqrt{\pi}}\right]\frac{1}{\sqrt{a_c}} \quad (1)$$

In Eq. (1), the strength is inversely proportional to the square root of the defect size. Furthermore, Llorca et al. [7] predict that the critical defect size a_c is close to the average phase size in the eutectic structure, particularly at high growth speeds. Thus, higher strength of eutectic ceramics could be achieved by refining microstructure which accompanies with the reducing of flaw sizes. The microstructure size relates to the melt inherent properties (such as melt viscosity and homogeneity) and ambient conditions (such as cooling rate, heterogeneous nucleation sites).

In the present work, the preparation of eutectic ceramic processing a combination of large dimension and fine microstructure was examined using cooling method with moderate temperature gradients. The microstructure refinement behavior of Al_2O_3/ZrO_2/YAG was investigated by changing technological

*Corresponding author. Tel.: +86 0411 84707970; fax: +86 411 84709967.
E-mail address: gqchen@dlut.edu.cn (G.Q. Chen).

0272-8842/$ - see front matter © 2013 Elsevier Ltd and Techna Group S.r.l. All rights reserved.
http://dx.doi.org/10.1016/j.ceramint.2013.02.089

Table 1
Chemical composition of designed $Al_2O_3/ZrO_2/YAG$ ceramics in $Al_2O_3–ZrO_2–Y_2O_3$ ternary system.

Composition	Al_2O_3 (mol%)	Y_2O_3 (mol%)	ZrO_2 (mol%)
Hypoeutectic (E_{01})	69.5	16	14.5
Hypoeutectic (E_{02})	65	18	17
Eutectic (E_0)	65	16	19
Hypereutectic (E_{03})	64	16	20

conditions in respect of ceramic composite, cooling rate, heterogeneous nucleation sites and melt superheating treatment.

2. Experimental procedures

2.1. Precursor and composition

According to the $Al_2O_3–ZrO_2–Y_2O_3$ ternary system [12], Al_2O_3/ZrO_2 (YSZ)/YAG nanocomposite powders with designed compositions were prepared by using a liquid-phase co-precipitation method. The powders were spark-plasma sintered into Al_2O_3/ZrO_2/YAG green compacts (Φ 10–15 mm) at 1450 °C for 10 min under 30 MPa. There are four designed compositions for examination, as shown in Table 1, two of them are hypoeutectic compositions E_{01} and E_{02}, the other two are eutectic composition E_0 and hypereutectic composition E_{03}.

2.2. Cooling rate

The green compacts with eutectic composition were melted in a vacuum chamber, and then were solidified by quenching and with controlled cooling rates of 10, 50, and 250 °C/min, respectively. The melt was heated to 1800 °C and held for 30 min. For the quenching process, the precursor rods were melted by electron beam on a graphite plate cooled by water. The spherical arc-melted specimen was quenched by shutting off the electron beam.

2.3. Melt superheating treatment

Al_2O_3/ZrO_2/YAG green compacts with eutectic composition were melted in Mo crucible and heated to a predetermined temperature T_s (the melt superheating temperature), ranging from 1750 °C to 2000 °C, and held for about 60 min. The melt was then cool down to the temperature of 1750 °C and held for 5 min to make melt temperature even, and finally was solidified to room temperature with a cooling rate of 10 °C/min. Fig. 1 shows the appearance of melt-grown Al_2O_3/ZrO_2/YAG rod with a diameter of 10 mm, which has a shrinkage cavity in the center.

3. Results and discussion

3.1. Compositions

Fig. 2 shows the solidification micrographs of Al_2O_3/ZrO_2/YAG ternary ceramics with different compositions. Based on

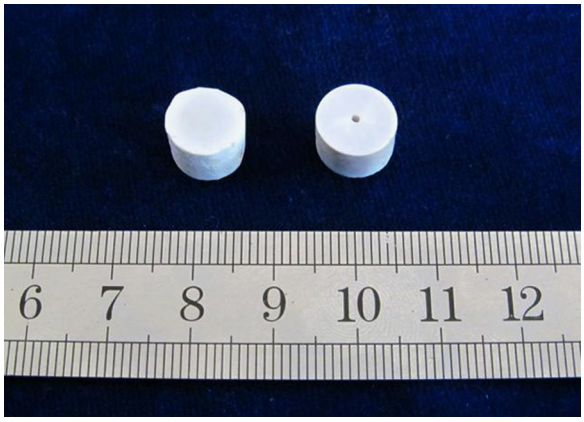

Fig. 1. Appearance of spark-plasma sintered precursor (left) and melt-grown eutectic rod (right) of Al_2O_3/ZrO_2/YAG ceramics.

X-ray diffraction (XRD) and energy-dispersive X-ray spectrometry (EDS), the components of rods are identified as α-Al_2O_3, YAG and cubic ZrO_2 (YSZ). In SEM micrographs, the components can be distinguished by the gray level, i.e. the gray matrix region is YAG, the black region is α-Al_2O_3, and the white region is cubic YSZ (a small amount of Y_2O_3 dissolved in the ZrO_2 phase). Fig. 2(a) is the microstructure of sample with hypoeutectic composition E_{01}. It is a typical off-eutectic microstructure, consisting of a coarse primary Al_2O_3/YAG binary eutectic and a fine Al_2O_3/ZrO_2/YAG ternary eutectic. The microstructure indicates the solidification path of the melt with the composition E_{01} deviates from Al_2O_3/ZrO_2/YAG coupled eutectic growth zone to Al_2O_3/YAG binary eutectic area. During solidification, the eutectic reaction of Al_2O_3/YAG first takes place from the melt and grows up with the composition of remaining liquid shifting to the Al_2O_3/ZrO_2/YAG coupled eutectic zone until Al_2O_3/ZrO_2/YAG ternary eutectic reaction occurs. In contrast to the hypoeutectic composite E_{01}, the microstructure of samples with compositions of E_{02}, E_0, and E_{03} all shows a typical irregular ternary eutectic structure, as shown in Fig. 2(b, c, d). Meanwhile, the microstructure with hypereutectic composition E_{03} is obviously finer than others due to higher content of ZrO_2 which increases the melt viscosity and reduces the growth length scale during solidification. Furthermore, examinations of solidification microstructure come across a primary phase of YAG in hypoeutectic E_{02} and a primary phase of ZrO_2 in hypereutectic E_{03}, respectively, as shown in Fig. 3. This phenomenon reveals that compositions of E_{02} and E_{03} locate in

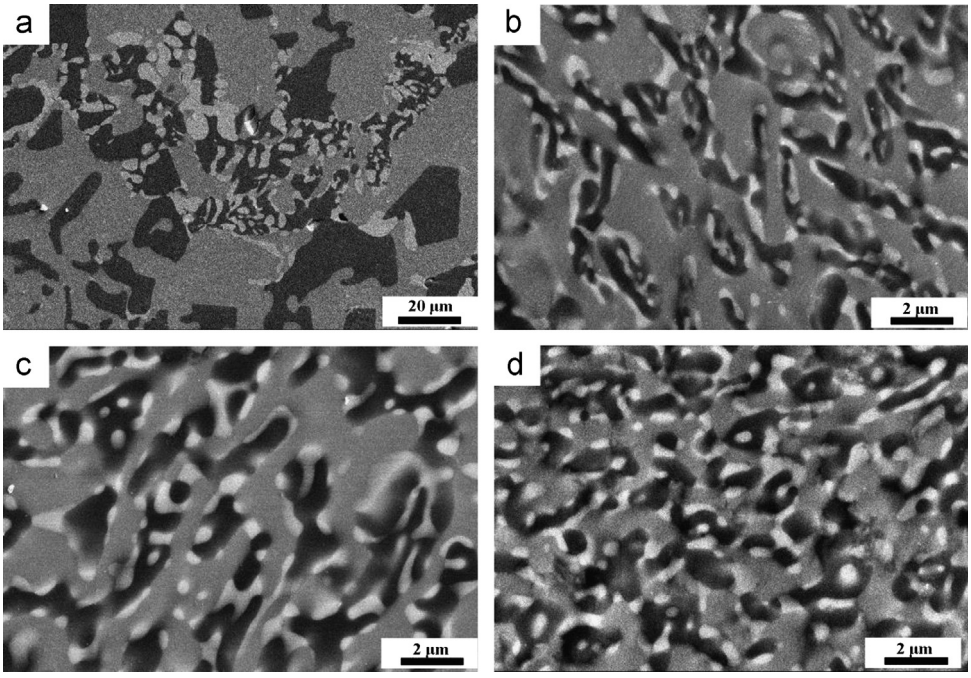

Fig. 2. Micrographs of Al_2O_3/ZrO_2/YAG solidification samples with different compositions: (a) hypoeutectic E_{01}; (b) hypoeutectic E_{02}; (c) eutectic E_0; and (d) hypereutectic E_{03}.

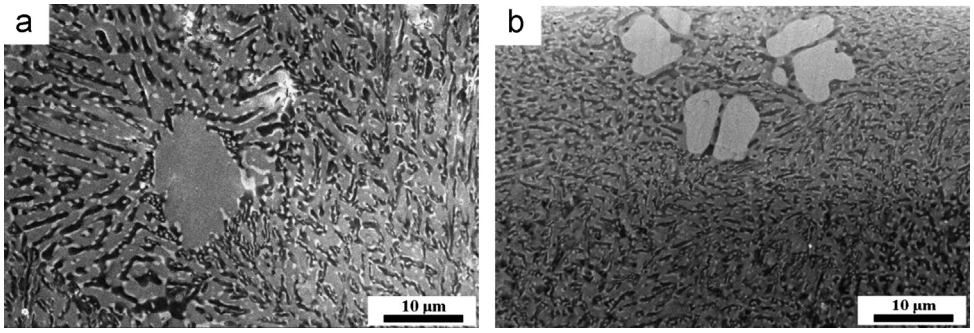

Fig. 3. Primary phase of YAG (a) and ZrO_2 (b) appearing in samples with compositions of hypoeutectic E_{02} and hypereutectic E_{03}, respectively.

the boundary of the Al_2O_3/ZrO_2/YAG ternary coupled eutectic zone.

3.2. Rapid cooling

Fig. 4 shows the solidification micrographs of Al_2O_3/ZrO_2/YAG samples grown under different cooling rates. The microstructure has a major variation in both the phase size and the morphology characteristic with the increase of cooling rate. Under lower cooling rates of 10 and 50 °C/min, the microstructure is made up of colonies, as shown in Figs. 4(a) and (b). The colony structure is not homogenous, i.e. the colony core is fine eutectic structure and the intercolony region contains coarse Al_2O_3 and ZrO_2 blocks. The colony diameter and the intercolony region become smaller at the higher cooling rate. By comparison, the phase size (or interspacing) of samples grown at cooling rates of 10 and 50 °C/min is close to that of ones prepared by laser-heated floating-zone method at growth rates of 10 mm/h and 50 mm/h, respectively [3]. With increasing the cooling rate to 250 °C/min, the solidification structure changes to coarse dendrites, as shown in Fig. 4 (c). The dendrite morphology seems like a combination of the Al_2O_3 and YAG phases, whereas the ZrO_2 phase distributes at the tip of the dendrites. The occurrence of dendrite relates to non-equilibrium solidification. Under rapid cooling, eutectic composition point moves to higher content of ZrO_2 phase with highest melting point among the components. The melt with composition E_0 therefore becomes hypoeutectic one which is easy to generate dendrite structure due to the constitutional supercooling [13]. In addition, some long strip or irregular round shape ZrO_2 blocks were observed among dendrites, as shown in Fig. 5(a). In some ZrO_2 blocks, interfaces indicated by red arrows in Fig. 5(b) are found. This indicates the large ZrO_2 blocks may result from the gathering of the small ZrO_2 particles at the tip of dendrite. For the quenching sample, its morphology characteristic is that of a fibrillar eutectic cell, instead of dendrite or irregular eutectic colony, as shown in Fig. 4(d). In the cell, parallel nano-scale Al_2O_3 and ZrO_2 rods

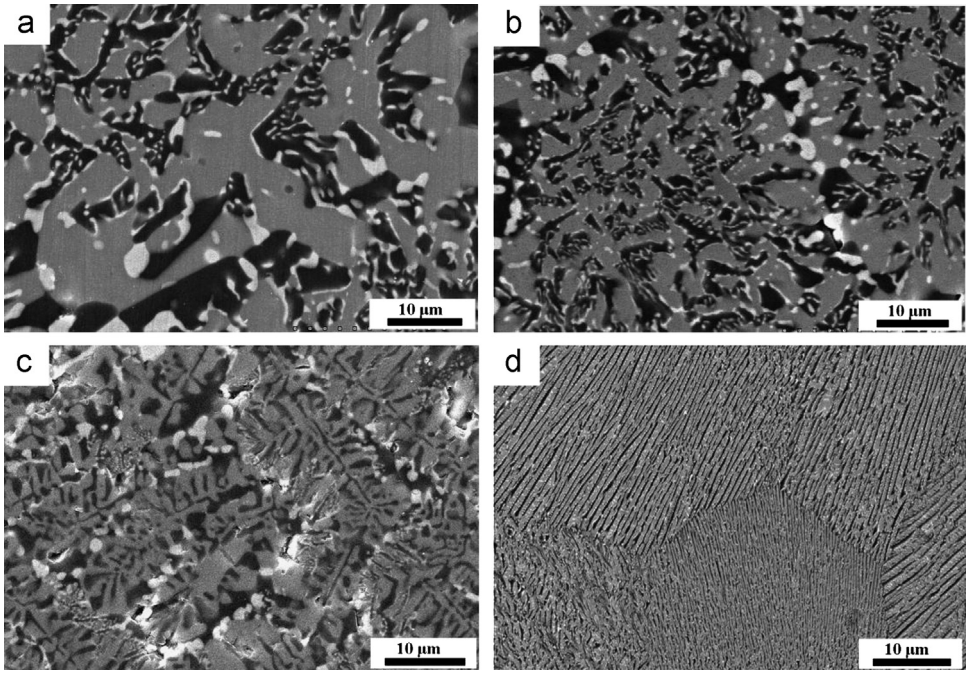

Fig. 4. Solidification microstructure of Al_2O_3/YAG/ZrO_2 ceramic with eutectic composition under different cooling rates: (a) 10 °C/min; (b) 50 °C/min; (c) 250 °C/min; and (d) quenching.

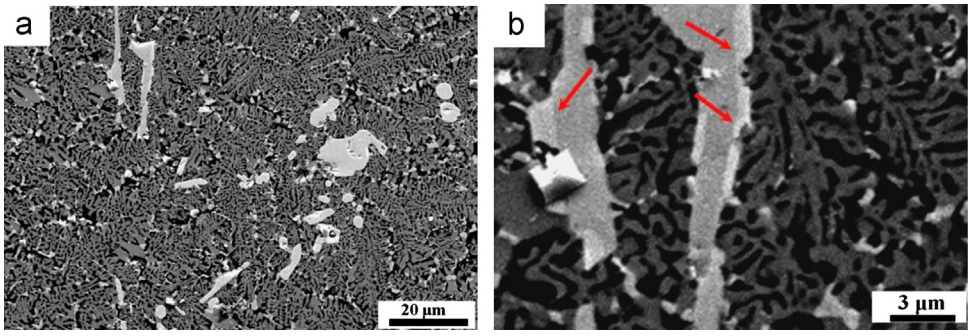

Fig. 5. ZrO_2 blocks appearing in the dendrite structure sample grown under the cooling rate of 250 °C/min (a); the detailed microstructure of long strip ZrO_2 blocks (b). There are some interfaces in the ZrO_2 block indicated by red arrows. It suggests the large block is a combination of small pieces ZrO_2 at tips of dendrites. (For interpretation of the references to color in this figure legend, the reader is referred to the web version of this article.)

are densely embedded in the crystal matrix of YAG, and the interphase spacing of Al_2O_3/ZrO_2/YAG eutectic is in submicron level. But on the surface layer of the quenching sample, the microstructure is complex and fundamentally different from the inside one, as shown in Fig. 6. There are many primary ZrO_2 dendrites and Al_2O_3/ZrO_2 eutectic zones, which are surrounded by coarse Al_2O_3/ZrO_2/YAG eutectic, as seen in Fig. 6(a). Moreover, it was identified in high magnification micrograph that some light gray zones appear in the dark gray zones of YAG, as shown in Fig. 6(b). EDS analysis in Fig. 6 reveals the composition of the light gray zone close to that of the metastable YAP phase. During EDS test, the energy of the incident electrons is 15 KV, and the working distance (WD) is 9 mm. The YAP existence may demonstrate that the temperature on the surface of the undercooled melt is lower than 1650 °C(the metastble eutectic point E_S), which favors YAP nucleation. Whereas the Al_2O_3/ZrO_2/YAG eutectic structure inside of the sample implies the temperature of undercooled melt (inside) is higher than 1650 °C, which causes the annealing of the generated YAP crystal and the transformation of partial zones of YAP phase into YAG phase. The formations of primary ZrO_2 dendrites and Al_2O_3/ZrO_2 eutectic zones ascribe to the eutectic composition of undercooled melt deviating from the metastable eutectic composition E_S to the Al_2O_3/ZrO_2 binary eutectic area.

In Fig. 4, the phase size of Al_2O_3/ZrO_2/YAG eutectic decreases with an increase in cooling rate. According to Jackson–Hunt model, during eutectic couple growth the interphase spacing λ, the undercooling ΔT at the solid–liquid interface and the crystal growth velocity V have a relationship as follows [1]:

$$\Delta T = K_1 \lambda V + K_2/\lambda \tag{2}$$

$$\lambda^2 V = K_2/K_1 = K \tag{3}$$

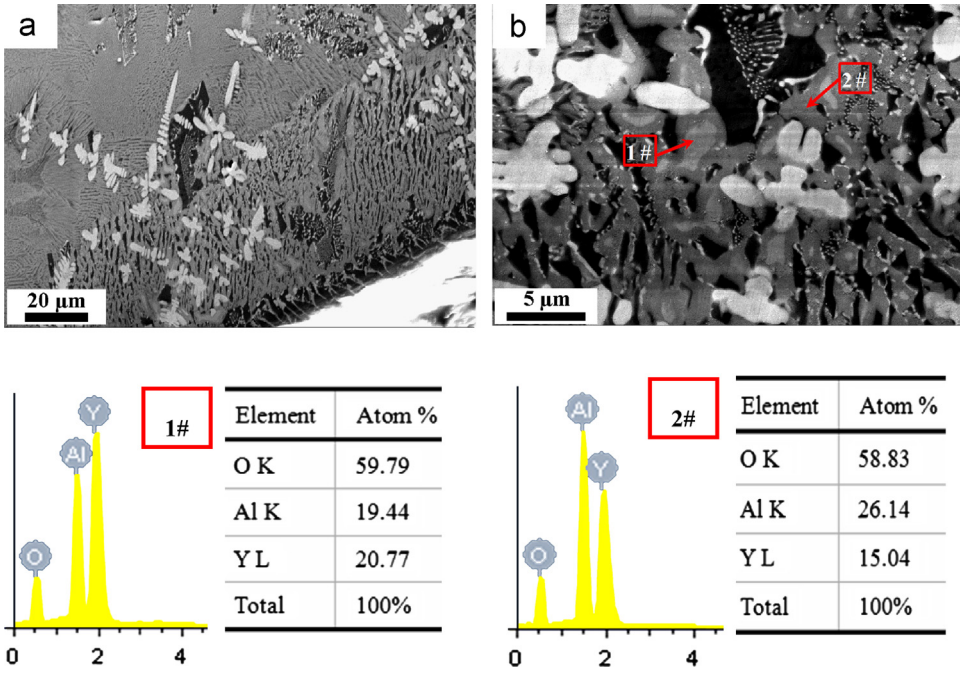

Fig. 6. Microstructure and EDS analysis on the surface layer of the quenching sample of Al_2O_3/ZrO_2/YAG ceramic.

where K_1 and K_2 are constants. From formulas (2) and (3), it can be deduced that the relation between the undercooling $\Delta T$and the interphase spacing λ is $\Delta T = \frac{2K_2}{\lambda}$. Meanwhile, the nucleation undercooling ΔT of eutectic melts increases with the cooling rate $\dot{T}$, i.e. $\Delta T \propto \dot{T}$ [14–15] because faster cooling will lower the melt temperature before nucleation occurring by accelerating heat transfer, schematically shown in Fig. 7. Hence, it can be concluded that the interphase spacing λ decreases with the increase of cooling rate $\dot{T}$ during eutectic growth, i.e. $\dot{T} \propto \frac{1}{\lambda^2}$, which agrees well with the actual experimental result in Fig. 4.

The evolutions of solidification structure are closely related to the morphology of solid–liquid interface [16]. The colony, dendrite and cell structures in Fig. 4 are corresponding to cellular, dendrite and cellular morphologies of solid–liquid interfaces, respectively. The transition sequence of solidification microstructure in Fig. 4 agrees very well with the trend of morphology variation of solid–liquid interfaces with the increase of growth rate. The morphology variation of the solid–liquid interface is the interplay result between solute diffusion and the curvature effects [15].

3.3. Melt superheating treatment

Fig. 8 shows the solidification microstructure of ceramic rods solidified in Mo crucible after melt superheating treatment at different temperatures. The microstructure varies significantly as a function of melt superheating temperature, in both the structure and the morphology. Under the melt superheating temperatures of 1800 °C and 1850 °C, the morphology is the typical irregular Al_2O_3/ZrO_2/YAG eutectic and the phase size is much finer at the higher temperature, as shown in Fig.8 (a) and (b). However, the solidification morphology becomes coarse and complex after melt superheating treatment at 1900 °C and 1950 °C,

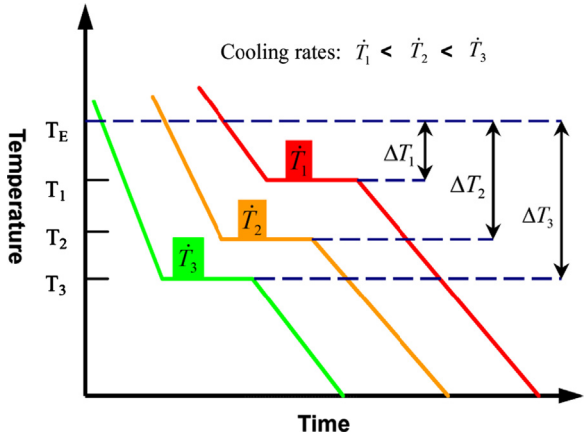

Fig. 7. Schematic diagram of a relationship between cooling rate and crystallization temperature.

as seen in Fig. 8(c) and (d). Based on XRD analysis, components of the complex microstructure are identified as α-Al_2O_3, metastable YAP, and cubic ZrO_2 phase, as shown in Fig. 9. The metastable microstructure is not uniform, consisting of a fine Al_2O_3–ZrO_2 eutectic structure and a coarse Al_2O_3–ZrO_2–YAP metastable structure. But the microstructure distribution has regularity that the fine Al_2O_3–ZrO_2 eutectic is always surrounded by the coarse Al_2O_3–ZrO_2–YAP metastable structure. The same metastable microstructure feature has been reported by Mizutani et al. [17] who suggest that Al_2O_3–ZrO_2 and Al_2O_3–ZrO_2–YAP eutectic reactions occur successively during the solidification process.

To research heterogeneous catalysis of solidification, a tungsten (W) wire was placed in the bottom of Mo crucible. Fig. 10 shows the solidification microstructure of Al_2O_3/ZrO_2/YAG eutectic rods solidified with W wire under different melt

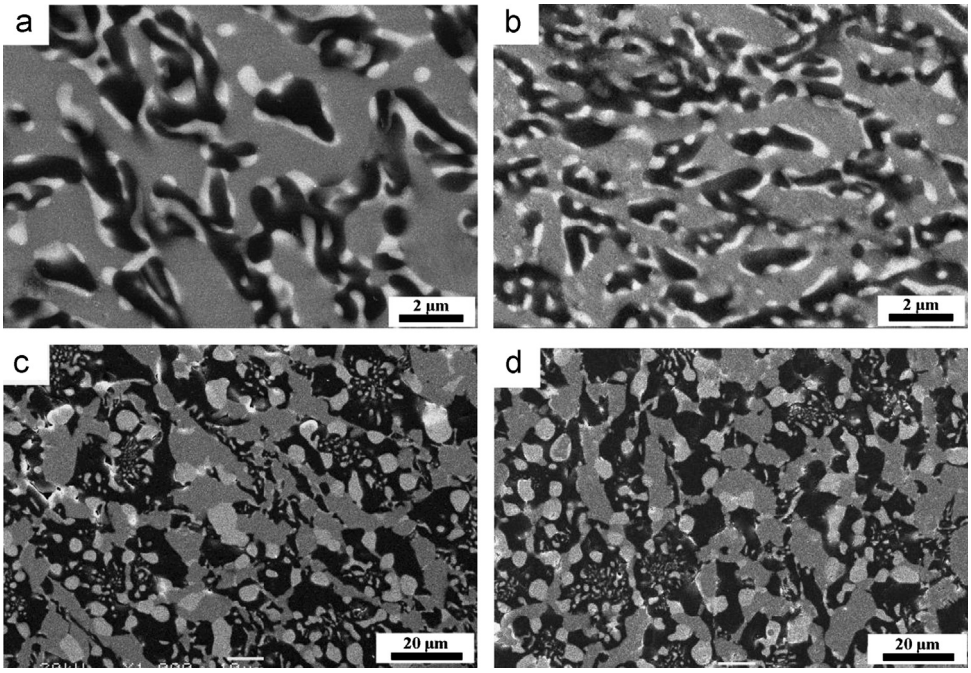

Fig. 8. SEM micrographs of ceramic rods grown in a Mo crucible as a function of melt superheating temperature: (a) 1800 °C; (b) 1850 °C; (c) 1900 °C; and (d) 1950 °C.

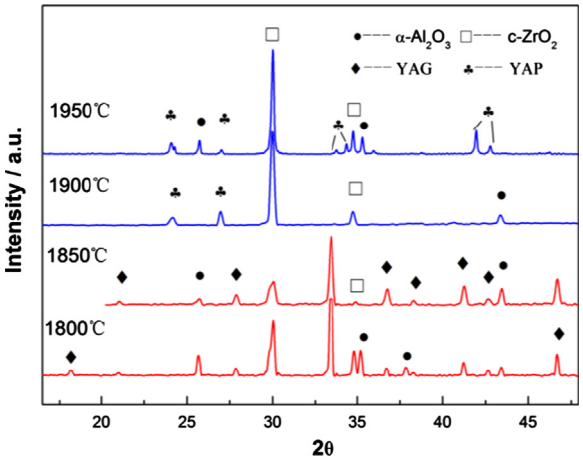

Fig. 9. XRD patterns of samples solidified in a Mo crucible under different melt superheating temperatures ranging from 1800 °C to 1950 °C.

superheating temperatures ranging from 1800 °C to 1950 °C. XRD analysis identified all the samples consisted of α-Al_2O_3, YAG, and cubic ZrO_2, no traces of metastable phases (YAP, YAM) or amorphous phase were detected. With the increase of melt superheating temperature, the Al_2O_3/ZrO_2/YAG eutectic microstructure refines dramatically and the morphology changes from irregular shape to parallel fibrous one. Under the melt temperatures of 1800, 1850 and 1900 °C, the solidification microstructure is the typical irregular Al_2O_3/ZrO_2/YAG eutectic. The microstructure scale of samples grown at melt superheating temperatures of 1800 and 1850 °C is almost alike and approaches that of sample grown at a growth speed of 60 mm/h by micro-pulling-down method [5]. Moreover, the phase size of sample solidified at the temperature of 1900 °C shows no difference from that obtained at a speed 100 mm/h by using laser directional processing [18]. Under the melt temperature of 1950 °C, the morphology changes to parallel fibrous Al_2O_3/ZrO_2/YAG eutectic. The morphology change of Al_2O_3/ZrO_2/YAG eutectic relates to the fact that the tendency to form faceted phases is reduced when the solidification rate is raised [19]. The interspacing size of the fibrous eutectic is closed to that prepared by laser directional solidification at a growth rate of 1200 mm/h [20].

Microstructure evolutions with the melt superheating temperature in Figs. 8 and 10 attribute to the variation of melt nucleation undercooling. This can be interpreted using the classical nucleation theory, which depicts the formation of a nucleus of critical r_k requiring activation energy ΔG_c [21].

$$r_k = \frac{2\sigma}{\Delta G} = \frac{2\sigma T_E}{L_m \Delta T} \tag{4}$$

$$\Delta G_c = \frac{16\pi\sigma^3}{3\Delta G^2} \cdot f(\theta) = \frac{4\pi\sigma}{3} \cdot r_k^2 \cdot f(\theta) \tag{5}$$

where, ΔG is the Gibbs free energy difference between the solid and the liquid phase, σ is the energy of the solid–liquid interface, T_E is the melting point, $f(\theta)$ is a catalytic potency factor of heterogeneous nucleation, and θ is the wetting angle. The function $f(\theta)$ is given by $f(\theta) = \frac{1}{4}(2-3cos\theta+cos^3\theta)$, where $0^\circ \le \theta \le 180^\circ$. Here, the onset of nucleation and the level of undercooling are controlled by heterogeneous catalysis.

At higher melt superheating temperature, the heterogeneous nucleation sites will be passivated along with the increase of wetting angle θ, which will enhance the activation energy threshold and decrease the nucleation rate. Therefore, increasing

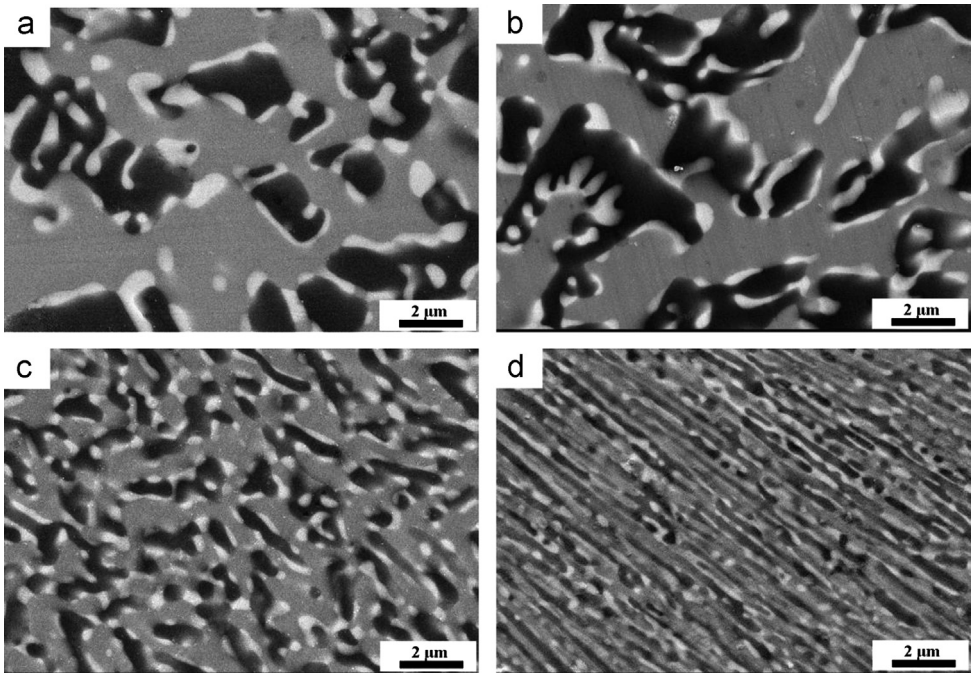

Fig. 10. SEM micrographs of Al_2O_3/YAG/ZrO_2 eutectic rods solidified with a seed crystal of W as a function of melt superheating temperature: (a) 1800 °C; (b) 1850 °C; (c) 1900 °C; and (d) 1950 °C.

the melt undercooling level is necessary to reduce the activation energy ΔG_c.

Under the same melt superheating temperature, the microstructure of samples solidified in Mo crucible (first case) shown in Fig. 8 is different from that of ones grown with a crystal seed of W wire (second case) in Fig. 10. At the lower melt superheating temperatures of 1800 °C and 1850 °C, the microstructure of Al_2O_3/ZrO_2/YAG eutectic in the first case is finer than the second one. At the higher melt superheating temperatures of 1900 °C and 1950 °C, the microstructure is Al_2O_3–ZrO_2–YAP metastable structure in the first case but Al_2O_3/ZrO_2/YAG eutectic structure in the second case. These differences demonstrate that the undercooling level of melt without placing W is larger. This is because W possesses higher melting temperature (3695 K) and better stability than Mo metal and is not easy to be passivated. Consequently, melt superheating treatment is a practicable method to produce eutectic ceramics with desired fine microstructure by controlling treatment conditions.

4. Conclusion

Melt-grown eutectic Al_2O_3/YAG/ZrO_2 ceramic rods were successfully prepared with diameter of 15 mm. The effects of composition, cooling rate, heterogeneous nucleation sites and melt superheating treatment on microstructure developments were investigated. The hypoeutectic ceramic with ZrO_2 content of 14.5 mol % consists of a coarse Al_2O_3/YAG eutectic and a fine Al_2O_3/YAG/ZrO_2 eutectic. As the ZrO_2 content range is 17–20% the solidification microstructure is a fine Al_2O_3/YAG/ZrO_2 eutectic and the phase size is smaller at a higher ZrO_2 content. With increasing the cooling rate, the solidification microstructure refines and the morphology develops as follows: from colony structure to dendrite structure, and then to cell structure. By melt superheating treatment, both the morphology and the components of solidification microstructure vary with superheating conditions. When the melt superheating temperature is equal or greater than 1900 °C, the microstructure of samples solidified in the Mo crucible is Al_2O_3–ZrO_2–YAP metastable structure. However, as the eutectic melt is solidified with a crystal seed of W wire the microstructure is parallel fibrous Al_2O_3/YAG/ZrO_2 eutectic at melt superheating temperature of 1950 °C.

Acknowledgments

This work was supported by the National Natural Science Foundation of China (Nos. 50875032 and 51175059), and also Supported by Program for New Century Excellent Talents in University (No. NCET-10–0278).

References

[1] J.L. Lorca, V.M. Orera, Directionally solidified eutectic ceramic oxides, Progress in Materials Science 51 (2006) 711–809.
[2] F.J. Ester, A. Larrea, R.I. Merino, Processing and microstructural study of surface laser remelted Al2O3–YSZ–YAG eutectic plates, Journal of the European Ceramic Society 31 (2011) 1257–1268.
[3] J.I. Peña, M. Larsson, R.I. Merino, I. de Francisco, V.M. Orera, J. L. Lorca, J.Y. Pastor, A. Martín, J. Segurado, Processing, microstructure and mechanical properties of directionally-solidified Al_2O_3–$Y_3Al_5O_{12}$–ZrO_2 ternary eutectics, Journal of the European Ceramic Society 26 (2006) 3113–3121.
[4] D.Y. Park, J.M. Yang, Effect of the microstructure on the mechanical properties of a directionally solidified $Y_3Al_5O_{12}$/Al_2O_3 eutectic fiber, Journal of Materials Science 36 (2001) 5593–5601.

[5] J.H. Lee, A. Yoshikawa, Y. Murayama, Y. Waku, S. Hanada, T. Fukuda, Microstructure and mechanical properties of $Al_2O_3/Y_3Al_5O_{12}/ZrO_2$ ternary eutectic materials, Journal of the European Ceramic Society 25 (2005) 1411–1417.
[6] N. Nakagawa, H. Ohtsubo, A. Mitani, K. Shimizu, Y. Waku, High temperature strength and thermal stability for melt growth composite, Journal of the European Ceramic Society 25 (2005) 1251–1257.
[7] J.Y. Pastor, J. Llorca, A. Salazar, P.B. Oliete, I. de Francisco, J.I. Peña, Mechanical properties of melt-grown alumina–yttrium aluminum garnet eutectics up to 1900 K, Journal of the American Ceramic Society 88 (2005) 1488–1495.
[8] T. Mah, T.A. Parthasarathy, L.E. Matson, Processing and mechanical properties of $Al_2O_3/Y_3Al_5O_{12}$(YAG) eutectic composite, Ceramic Engineering and Science Proceedings 11 (1990) 1617–1627.
[9] S. Ochiai, T. Ueda, K. Sato, M. Hojo, Y. Waku, N. Nakagawa, S. Sakata, A. Mitani, T. Takahashi, Deformation and fracture behavior of an Al_2O_3/YAG composite from room temperature to 2023 K, Composites Science and Technology 61 (2001) 2117–2128.
[10] J.C. Newman, I.S. Raju, An empirical stress-intensity factor equation for the surface crack eng, Fracture Mechanics 15 (1981) 185–192.
[11] M.C. Mesa, P.B. Oliete, V.M. Orera, J.Y. Pastor, A. Martín, J. Llorca, Microstructure and mechanical properties of $Al_2O_3/Er_3Al_5O_{12}$ eutectic rods grown by the laser-heated floating zone method, Journal of the European Ceramic Society 31 (2011) 1241–1250.
[12] S.M. Lakiza, L.M. Lopato, Stable and metastable phase relations in the system alumina–zirconia–yttria, Journal of the American Ceramic Society 80 (1997) 893–902.
[13] H. Su, J. Zhang, K. Song, L. Liu, H. Fu, Rapid solidification and fracture behavior of ternary metastable eutectic Al_2O_3/YAG/YSZ in situ composite ceramic, Materials Science and Engineering A 528 (2011) 1967–1973.
[14] H. Ysduda, I. Ohnaka, Y. Mizutani, Y. Waku, Selection of eutectic systems in Al_2O_3–Y_2O_3 ceramics, Science and Technology of Advanced Materials 2 (2001) 67–71.
[15] G. Chen, X. Fu, J. Luo, Y. Zu, W. Zhou, Effect of cooling rate on the microstructure and mechanical properties of melt-grown Al_2O_3/YAG/ZrO_2 eutectic ceramic, Journal of the European Ceramic Society 32 (2012) 4195–4204.
[16] W. Kruz, D.J. Fisher, Fundamentals of Solidification, fourth ed., Trans. Tech. Publication, Switzerland, 1998.
[17] Y. Mizutani, H. Yasuda, I. Ohnaka, A. Sugiyama, S. Takeshima, M. Kirihara, Undercooled melt formation by melting of metastable eutectic structure in Al_2O_3–Y_2O_3–ZrO_2 system, Materials Transactions 43 (2002) 2847–2854.
[18] F.J. Ester, A. Larrea, R.I. Merino, Processing and microstructural study of surface laser remelted Al_2O_3–YSZ–YAG eutectic plates, Journal of the European Ceramic Society 31 (2011) 1257–1268.
[19] M. Cristina Mesa, P.B. Oliete, A. Larrea, V.M. Orera, Directionally solidified Al_2O_3–$Er_3Al_5O_{12}$–ZrO_2 eutectic ceramics with interpenetrating or nanofibrillar microstructure: residual stress analysis, Journal of the American Ceramic Society 95 (2012) 1138–1146.
[20] P.B. Oliete, J.I. Peña, A. Larrea, V.M. Orera, J. LLorca, J.Y. Pastor, A. Martín, J. Segurado, Ultra-high-strength nanofibrillar Al_2O_3–YAG–YSZ eutectics, Advanced Materials 19 (2007) 2313–2318.
[21] M. Herlach, Non-equilibrium solidification of undercooled metallic melts, Materials Science and Engineering R 12 (1994) 177–272.